Available online at www.sciencedirect.com
SCIENCE DIRECT®
ELSEVIER
International Journal of Multiphase Flow 29 (2003) 1857–1874
International Journal of Multiphase Flow
www.elsevier.com/locate/ijmulflow

Single bubble growth in saturated pool boiling on a constant wall temperature surface

Han Choon Lee [a], Byung Do Oh [a], Sung Won Bae [b], Moo Hwan Kim [a,*]

[a] *Department of Mechanical Engineering, Pohang University of Science and Technology, San 31, Hyoja-dong, Namgu, Pohang, Kyoungbuk 790-784, South Korea*

[b] *Korea Atomic Energy Research Institute, Duckjin-dong, Yusunggu, Taejon 305-353, South Korea*

Received 9 June 2003; received in revised form 25 September 2003

Abstract

Nucleate pool boiling experiments with constant wall temperatures were performed using R11 and R113 for saturated pool boiling conditions. A microscale heater array and Wheatstone bridge circuits were used to maintain a constant wall temperature condition and to obtain measurements with high temporal and spatial resolution. Accurate heat flow rate data were obtained from microscale heater array by controlling the surface conditions at a high temporal resolution. Images of the bubble growth were captured using a high-speed CCD camera synchronized with the heat flow rate measurements. The geometry of the bubble was obtained from the images. In the asymptotic growth region, the bubble showed a growth rate that was proportional to $t^{1/5}$, which was slower than the growth rate proposed in previous analytical analyses. The bubble growth behavior was analyzed using a new dimensionless parameter to permit comparisons with previous results at the same scale. The comparisons showed good agreement in the asymptotic growth region. A non-dimensional correlation for the bubble radius that can predict the bubble growth and the heat flow rate simultaneously, was suggested. The required heat flow rate for the volume change of the observed bubble was estimated to be larger than the instantaneous heat flow rate measured from the wall. Heat, other than the instantaneous heat supplied from the wall, is estimated to be transferred through the interface between bubble and liquid, even with saturated pool conditions. This phenomenon under a saturated pool condition needs to be analyzed and the data from this study can supply the good experimental data with the precise boundary condition (constant wall temperature).

Keywords: Saturated pool boiling; Constant wall temperature; Single bubble growth; Microscale heater array

* Corresponding author. Tel.: +82-54-279-2165; fax: +82-54-279-3199.
E-mail address: mhkim@postech.ac.kr (M.H. Kim).

0301-9322/$ - see front matter © 2003 Elsevier Ltd. All rights reserved.
doi:10.1016/j.ijmultiphaseflow.2003.09.003

1. Introduction

A study of partial nucleate boiling is important in order to understand the overall characteristics of boiling phenomena. Since an analytical description of the phenomena requires complex interfacial modeling, theoretical approaches have been simplified using assumptions, and studies at physical scales have been performed experimentally, in the main (see Dhir, 1998, for a succinct review). Previous investigations of partial nucleate boiling can be divided into groups according to the pool temperature (superheated, saturated, and subcooled boiling) and wall heating conditions (constant wall temperature and constant heat flux). In this study, a saturated pool boiling experiment was performed using constant wall temperatures to analyze single bubble growth without the effect of superheat or subcooled. The results include the instantaneous heat flow rate supplied from the heating wall and bubble growth images.

Most of the previous research on single bubble growth has been performed using a constant wall heat flux created by heating a metallic block beneath the bubble. However, the constant heat flux condition is estimated to be distorted because of the conduction in the heating block and wall condition. The few previous experiments on saturated boiling found in the literature (Staniszewski, 1959; Han and Griffith, 1965; Cole and Shulman, 1966) did not show good repeatability for bubble growth, even in a series of data with the same experimental conditions. In this paper, we show that the local heating power should be controlled within a microsecond in order to maintain the same heating conditions during the inception of a bubble; this requirement may be related to the irregular behavior of the previous results.

Recently, Rule et al. (1998) developed a microscale heater array that can be controlled at a high temporal and spatial resolution. A constant wall temperature can be achieved using the microscale heater array, and variation in the heat flow rate for a single bubble can be measured. Using the heater array, Rule and Kim (1999), Kim and Benton (2002) and Kim et al. (2002) performed various subcooled boiling experiments by varying the gravity condition under constant wall temperatures. In this study, the same heater array is used to maintain a constant wall temperature and to measure the heat flow rate. Since the heat flow rate to the bubble during growth is a fundamental question in this field, precise measurement is of great interest.

Analytical analyses for the growth of a single bubble have been performed for simple geometric shapes, using a simplified heat transfer model, because of the complexity of the phenomena. Rayleigh (1917) suggested an equation of motion for a spherical bubble governed by the momentum interaction between the bubble and the liquid around the bubble; heat transfer through the bubble interface is not considered. The result gives the high growth rate that is observed during the initial growth region (or inertia-controlled region). Plesset and Zwick (1954) and Forster and Zuber (1954) solved the Rayleigh equation by considering the heat transfer through the bubble interface in a uniformly superheated liquid. The bubble growth equation was obtained from the heat conduction through the thermal boundary layer around the bubble. They derived the temperature gradient at the interface using the thin thermal boundary layer approximations and by assuming a uniformly superheated bulk liquid. Robinson and Judd (2001) reported that the heat could be supplied through the bubble interface except the bottom surface by the interface cooling effect, even under a saturated pool condition. The interface cooling effect was reported also by the earlier researchers (Plesset and Zwick, 1954; Zuber, 1961; Mikic and Rohsenow, 1969).

It is the most important factor to identify the thermal boundary layer around a bubble. But it is very difficult to measure the temperature field around a bubble. In this study, the heat flow rate behavior was indirectly and quantitatively analyzed by comparing the growth rate of bubble and the heat flow rate supplied through the bottom surface of a bubble. Since a bulk liquid is another heat source for bubble growth in a superheated or subcooled pool, as well as the thermal boundary layer grown from the heated wall, the present experiment is performed using a saturated pool to minimize the effect of superheat or subcooled. The bubble growth and departure behavior was measured with high speed CCD camera with a constant wall temperature condition. These data were analyzed and compared with the results from previous studies, using a new dimensionless parameter.

2. Experiments

2.1. Experimental apparatus

A microscale heater array was used to maintain a constant wall temperature. It was constructed on a transparent glass substrate using the VLSI technique. The Ti/Pt and Ti/Au layers were deposited using an electric beam evaporator to generate a heating surface and power leads. Each heater in the array had dimensions of 0.27×0.27 mm, which is comparable with the diameter of a typical single bubble, 0.25–0.7 mm. A description of the device, along with some of the results obtained, can be found in previous research by Rule et al. (1998), Rule and Kim (1999) and Bae et al. (1999). The roughness of the heating surface was around 0.4 μm that is the height of the heating line with respect to the base substrate. The static contact angle of the microscale heater array surface was 71° for distilled water, 30.9° for R11, and 11.4° for R113. Compared with the contact angle for distilled water, R11 and R113 showed more hydrophilic characteristics. The dynamic characteristics of a boiling bubble is supposed to be different with the static contact angle, but the result of the static contact angle measurement could give the expectation that a boiling bubble of R11 and R113 would have more spherical shape.

A typical characteristic timescale for the initial growth region is 10^{-6} s, as shown by the dimensional analysis in Section 3. Most of the experimental devices, that have been used previously to control the power of the heating block beneath a bubble and provided a constant heat flux, could not maintain the surface condition at an appropriately high temporal resolution. Therefore, severe deviations in the initial behavior of the observed bubble growth were observed. The present microscale heater array was controlled with Wheatstone bridge circuit. Among the parts of the circuit, the longest time delay occurs at the OP amp that has a time resolution of 10^{-7} s. Due to the fast control of the surface condition, good repeatability was achieved in the experimental results.

The temperature of each heater in the array was controlled by 96 electric Wheatstone bridge feedback circuits, in a manner similar to constant-temperature hot-wire anemometry. Each heater in the array can be represented as one resistor in a Wheatstone bridge circuit. The data acquisition system was capable of sampling 16,000 data points from each heater at a speed of 7.35 kHz with 12-bit resolution. The data acquisition system was synchronized with a high-speed CCD camera

system. A long distance microscopic lens was used to capture the small bubbles during boiling (see Figs. 1 and 2).

Fig. 1 shows a schematic diagram of the main boiling chamber. The chamber was designed to provide bottom and side views of bubble growth. An aluminum-deposited mirror was placed below the bottom surface of the main chamber to adjust the viewing line of the CCD camera. Ten thin film heaters providing 10 W/in^2 were attached to the side of the chamber to control the pool temperature for saturated pool boiling. A 250-W halogen lamp mounted near the sight window was used as a light source. A photograph of the experimental facility is shown in Fig. 2.

2.2. Calibration

Each heater in the array can be represented as one resistor in a Wheatstone bridge circuit, and the resistance of each heater varies with temperature. The resistances of the other resistors in the

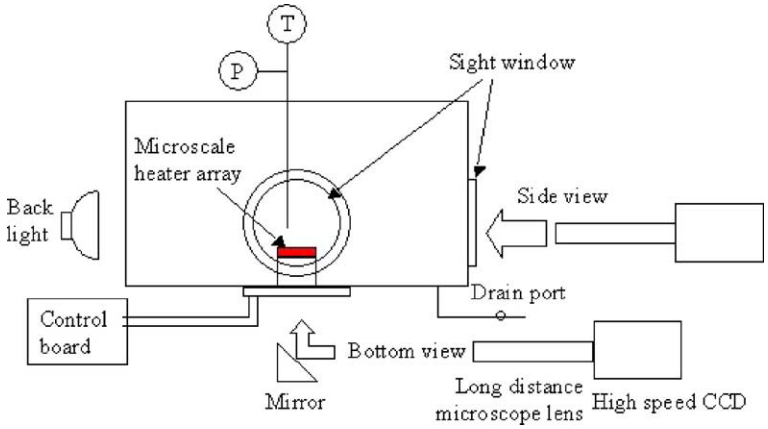

Fig. 1. Schematic diagram of the main chamber.

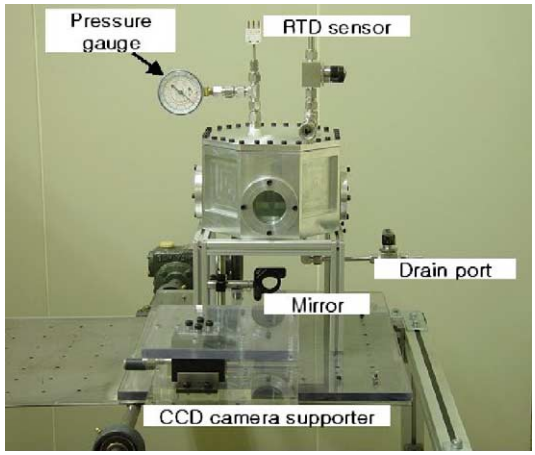

Fig. 2. Photograph of the experimental apparatus.

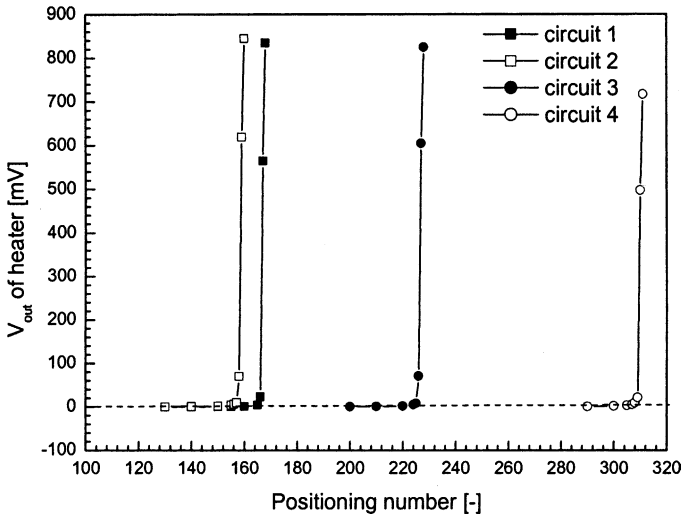

Fig. 3. Microscale heater output threshold behavior.

Wheatstone bridge are adjusted to balance the voltage on the two sides of the circuit. The resistances are controlled using a digital potentiometer. Thus, the resistance of the digital potentiometer, which corresponds to the resistance of a heater at a given temperature, must be calibrated. This requires maintaining the microscale heater array at a constant temperature, which is achieved by using a constant temperature bath containing olive oil.

Since the resistance of the digital potentiometer cannot be known a priori, it must be found by trial and error. Fig. 3 shows the threshold behavior of the digital potentiometer. The digital potentiometer in the Wheatstone bridge circuit had 512 digital positioning numbers for 0–20 kΩ. The abscissa in Fig. 3 represents the positioning number for controlling the digital potentiometer and the ordinate is the voltage output of heater. Each heater had a different threshold value. Near the equivalent point, a slight change in the potentiometer resistance caused an abrupt increase in the voltage output due to the resistance balance between the digital potentiometer and the heater in the Wheatstone bridge circuit. The calibration processes were conducted between 25 and 69 °C at intervals of about 2 °C. The maximum uncertainty of the calibrated temperature was 0.59 °C.

2.3. Uncertainty analysis

The observed bubble shape was almost axi-symmetric with respect to the axis normal to the heating surface and non-symmetric vertically. Thus, the equatorial radius (B) shown in Fig. 4 was not a good measure of the representative radius, although it has often been used with the truncated sphere assumption. Since most previous analytical analyses for bubble growth have been for a spherical bubble, growth behavior in the present study was analyzed using the equivalent radius of a sphere with the same volume. The bubble volume was calculated with the measured bubble dimensions in Fig. 4.

If the bubble is an axi-symmetric and is not symmetric vertically, then the bubble can be divided into two parts (upper and lower parts). Suppose that the upper portion of a bubble is a half of a

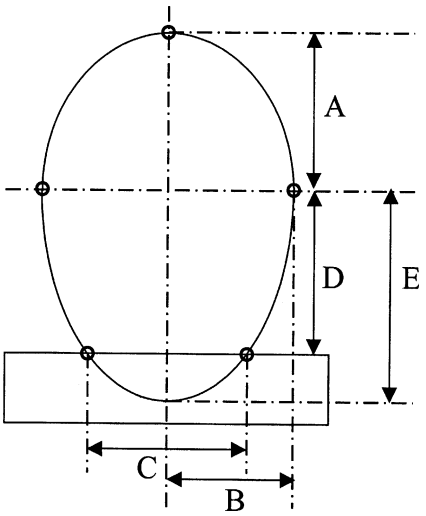

Fig. 4. Geometry of a spheroid.

spheroid. Then the volume of the upper portion (V_U) can be calculated using the dimensions of the polar and equatorial radii, A and B, in Fig. 4,

$$V_U = \frac{2}{3}\pi B^2 A. \tag{1}$$

The volume of the lower portion (V_L) can be calculated using B, D, and C (see Fig. 4),

$$V_L = \pi B^2 \left[D - \frac{D^3}{3E^2} \right], \qquad E = \sqrt{\frac{D^2}{1 - \frac{(C/2)^2}{B^2}}}. \tag{2}$$

The equivalent radius, R_{eq}, is defined as the radius for which the total volume (V) from the measurements is balanced with that of a sphere of equivalent radius,

$$V = V_U + V_L = \frac{4}{3}\pi R_{eq}^3, \qquad R_{eq} = \left(\frac{1}{2} B^2 A + \frac{3}{4} B^2 \left[D - \frac{D^3}{3E^2} \right] \right)^{\frac{1}{3}}. \tag{3}$$

The equivalent radius can be calculated with the measured dimensions in Fig. 4. The errors of the dimension measurement will propagate into the calculation of the equivalent radius. Dimensions of a bubble shown in Fig. 4 were measured by counting the number of pixels in a captured image. A micrometer was placed in the chamber to provide guidance for the size measurements. From the captured micrometer image at the same distance as the bubble nucleation, a physical dimension of 100 μm corresponds to 30 pixels for the cases of R11. One pixel in the image corresponds to 3.333 μm. For R113, 100 μm of the micrometer corresponds to 11 pixels and one pixel in the image corresponds to 9.091 μm. The captured images for R11 were not clear and the bubble dimensions could be measured with the maximum error of ±2 pixels error, whereas the clear images of R113 could be measured with the error of ±1 pixel. The uncertainty analysis was conducted by using the method explained in Coleman and Steele Jr. (1989). The uncertainty

analysis for R11 showed the maximum uncertainty of 3.6% at the first image that showed the smallest bubble and except the first image, they were smaller than 1.8%. For R113, maximum uncertainty of 6.7% occurs at the first image. Except the first images, however, the uncertainties were smaller than 3.4%.

The bubble inception time was predicted with the CCD camera time of the first image and the time of the heat flow rate data. Images of a bubble for R113 and R11 were taken with the time resolution of 0.25 ms (4000 frames/s) and 1 ms (1000 frames/s), respectively. The heat flow rate data from the microscale heater array were measured with the time resolution of 0.136 ms. In the present experiments, the inception time was chosen as the time right before the jump of the heat flow rate and the error of the inception time would be maximum 0.136 ms.

A thermocouple with 0.53 °C uncertainty was used to calibrate the temperature of the microscale heater array. The digital potentiometer in the Wheatstone bridge circuit had 512 digital positioning numbers. The Wheatstone bridge circuit was set to give a temperature displacement of 60 °C. Thus, 1 digit had a 0.12 °C temperature displacement and an uncertainty of 0.06 °C. The maximum uncertainty of the calibrated temperature was, therefore, estimated to be 0.59 °C, which was the sum of the errors of the thermocouple and digital potentiometer: 0.53 and 0.06 °C, respectively.

The voltage of each heater was measured using a 12-bit A/D system and the maximum voltage is 12 V. The digitizing bias error is, therefore, estimated to be ±0.0015 V. All of the heater output voltages measured, while a bubble was being generated, were above 2 V. That means the maximum uncertainty of the voltage measurement is ±0.075%.

3. Results and discussion

3.1. Experimental results of the bubble growth and heat flow rate

The nucleate pool boiling experiments were conducted under the atmospheric pressure (1 atm). Working fluids were R11 and R113, and the saturation temperature is 23.7 and 47.5 °C, respectively. The bulk liquid temperature was 23 and 47 °C, respectively, and it was almost saturated condition. The bubble growth and the heat flow rate behavior were measured under a constant wall temperature condition (35 °C for R11 and 61 °C for R113). The single bubble growth behavior was studied for the bubble that was not affected by the other bubbles. In the present experiment, only two nucleation sites were observed under the onset of nucleate boiling temperature (ONB temperature), and the distance between two sites was about 1.6 mm. It is about three times to the maximum bubble diameter.

The ONB temperature of 61 °C for R113 was found by varying the wall superheat. As expected, the lowest bubble frequency was observed for the ONB temperature condition. Fig. 5 shows side view images of a bubble for the wall temperature of 61 °C for R113. They were captured at a sampling rate of 4000 Hz, whereas 1000 Hz for R11. The bubble shown in Fig. 5 shows almost axi-symmetric shape with respect to the axis normal to the heating surface and non-symmetric shape vertically. To evaluate the equivalent bubble radius (Eq. (3)), the bubble shape was assumed to be an axi-symmetric and vertically non-symmetric. To confirm the assumption for the bubble shape shown in Fig. 4, the assumed bubble shape was compared with the actual bubble images in Fig. 5. The solid line in the graph overlaid in the images shows the assumed shape. It shows good

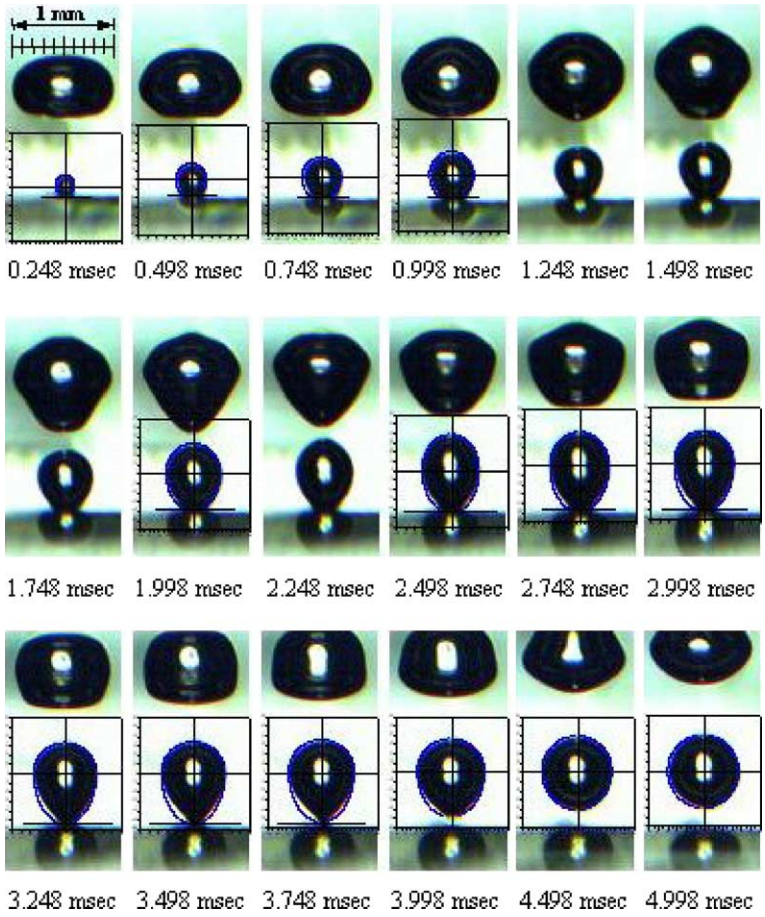

Fig. 5. Side view of bubble growth (R113, $T_{wall} = 61$ °C).

agreement with the actual shape during the bubble growth. Since the bubble shows the necking phenomena closing to the departure time, the difference between the assumed shape and the actual image appeared. The maximum difference is shown at the departure time of 3.748 ms. To evaluate the equivalent radius of the actual bubble, the coordinate of the bubble interface were measured and the volume was calculated by the integration with the interface coordinate. The equivalent radius evaluated from the actual volume at the departure time is 0.339 mm and the equivalent radius evaluated by the assumed shape at the same time is 0.352 mm. The maximum error of the assumed shape was estimated to be 3.8%.

In the present study, the instantaneous heat flow rate was measured on the heating surface, which was controlled at a constant temperature. Fig. 6 shows the heat flow rate data for a constant wall temperature for R11. The data were measured at a temporal resolution of 0.136 ms. There was an abrupt increase within 0.3 ms after inception. Afterwards, the heat flow rate decreased rapidly, except for a slight increase just before departure. The bubble departed completely after approximately 6 ms. In order to demonstrate the repeatability of the measurements of the instantaneous heat flow rate to the bubble, seven heat flow rate data starting from bubble in-

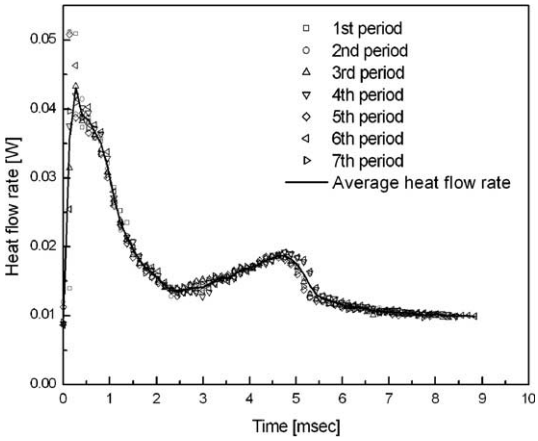

Fig. 6. Repeatability of the measured heat flow rate data.

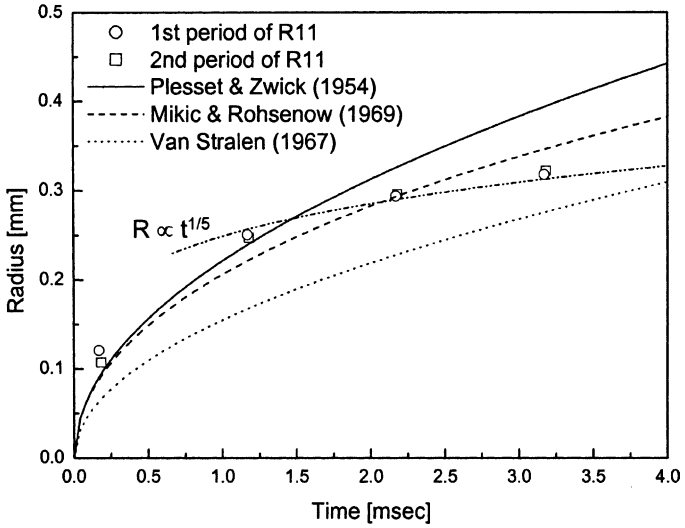

Fig. 7. Comparison of bubble growth with the previous predictions (R11, $T_{wall} = 35$ °C).

ception, were overlaid. Even though, due to the relatively low resolution of the data acquisition (not the temperature control of the heating wall) right after inception, there was a maximum deviation of 37% of the peak value of the heat flow rate. The overlaid data sets showed good repeatability with the maximum standard deviation less than 7%.

The equivalent radius is shown in Fig. 7, and is compared with previous analytical results. Plesset and Zwick (1954) assumed a uniformly superheated thermal boundary layer around a spherical bubble and predicted a $t^{1/2}$ asymptotic growth rate. Other predictions that modified the effective heat transfer area (Van Stralen, 1966) and the non-uniform temperature field around the bubble (Mikic and Rohsenow, 1969) still gave heat transfer areas that increased as the bubble grew, and an asymptotic growth rate of approximately $t^{1/2}$. However, the present results show a much slower growth rate that is proportional to $t^{1/5}$ after 1 ms.

The power of time for the bubble growth is intimately related with the heat flow rate behavior. To relate the heat flow rate to the equivalent radius, only the latent heat is assumed to change the bubble volume. This gives

$$\dot{q} = \dot{m} h_{fg} = 4\pi \rho_v h_{fg} R^2 \frac{dR}{dt}, \tag{4}$$

where $\dot{q}$ is the heat flow rate, $\dot{m}$ is the evaporating mass flow rate, h_{fg} is the latent heat of vaporization, ρ_v is the vapor density, R is the bubble radius, and t is the time. If the power of time for the bubble growth is less than one-third, the heat flow rate should decrease by the relation of Eq. (4). Since the power of the growth rate at the asymptotic growth region of the present experiment shows about one-fifth in Fig. 7, the heat flow rate should decrease with time (see Fig. 11(b)).

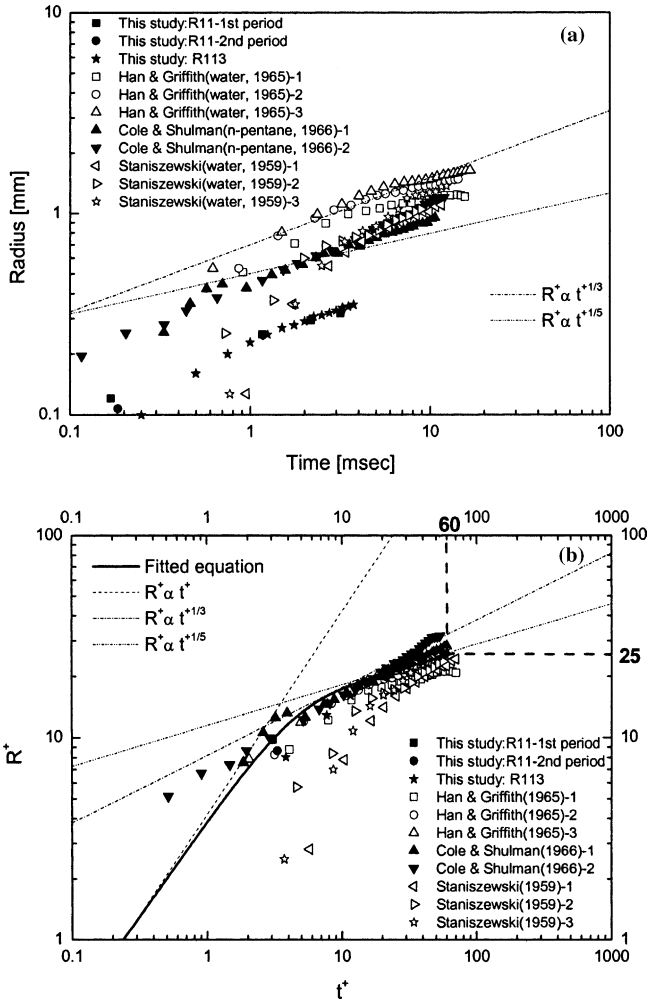

Fig. 8. Comparison of bubble growth with previous experimental results.

Fig. 8(a) shows a comparison of bubble growth with previous saturated pool boiling experimental results. In the previous experiments, water (Staniszewski, 1959; Han and Griffith, 1965) and *n*-pentane (Cole and Shulman, 1966) were used as the working fluids. A constant heat flux was applied at the heating surface. Both the present and previous experiments were performed in a pool at the saturation temperature under 1 atm. Previous experimental results for superheated pool boiling (see Lee and Merte Jr., 1996, for example) show that the asymptotic growth is proportional to $t^{1/2}$, which agrees well with the theoretical analysis. In saturated pool boiling, the asymptotic growth is proportional to between $t^{1/5}$ and $t^{1/3}$, as shown in Fig. 8(a). It is not quite clear how much the wall conditions affect the asymptotic growth rate, but there appears to be no discernable difference between the two different wall conditions. The heat flow rate remained approximately constant after about 1 ms (see Fig. 11(b)) in our constant wall temperature condition.

3.2. Dimensional analysis of the bubble growth and departure

Bubble growth and departure behavior shown in Fig. 8(a) is different with each fluid. In this study, dimensional analysis for bubble growth and departure was conducted. For dimensional analysis, characteristic time and length scale should be obtained.

The characteristic time scale can be determined from the ratio of the corresponding latent heat transfer and the conduction heat transfer rate through the interface,

$$\begin{aligned}\frac{q_{\text{latent}}}{\dot{q}_{\text{conduction}}} &= \frac{\rho_v h_{fg} \frac{4}{3}\pi R^3}{k_l 4\pi R^2 \dfrac{\partial T}{\partial r}} = \frac{1}{3}\frac{\rho_v h_{fg} R_c^3}{k_l R_c^2 \dfrac{T_c}{R_c}} \frac{R^{+3}}{R^{+2}\dfrac{\partial T^+}{\partial r^+}} = t_c \frac{R^+}{\dfrac{\partial T^+}{\partial r^+}},\\ t_c &= \frac{1}{3}\frac{\rho_v h_{fg} R_c^2}{k_l T_c} = \frac{1}{3}\frac{\rho_v h_{fg} R_c^2}{k_l \Delta T} = \frac{1}{3}\frac{1}{Ja\alpha} R_c^2,\end{aligned} \tag{5}$$

where k_l is the thermal conductivity of liquid, T is the temperature of liquid, and α is the thermal diffusivity of liquid. Since the bulk liquid is saturated and the bubble growth should be influenced by the wall superheat, the Jakob number is defined by $(\rho_l C_{Pl}\Delta T)/(\rho_v h_{fg})$ with the wall superheat ($\Delta T = T_{wall} - T_{sat}$) that is used as the characteristic temperature scale (T_c).

Suppose that bubble growth can be characterized by the pressure difference (ΔP) between the vapor and the bulk liquid pressures, the characteristic velocity scale (v_c) can be determined from the equation of motion (the extended Rayleigh equation)

$$\Delta P = P_v - P_\infty = \rho_l R\frac{d^2R}{dt^2} + \frac{3}{2}\rho_l\left(\frac{dR}{dt}\right)^2 + \frac{2\sigma}{R}, \tag{6}$$

$$v_c = \frac{R_c}{t_c} = \sqrt{\frac{2}{3}\frac{\Delta P}{\rho_l}}, \tag{7}$$

where ρ_l is the liquid density. Eq. (7) is almost same to the velocity scale of Mikic et al. (1970). From Eqs. (5) and (7), the characteristic radius and time scales are

$$R_c = \sqrt{\frac{27}{2}}Ja\alpha\sqrt{\frac{\rho_l}{\Delta P}}, \qquad t_c = \frac{9}{2}Ja\alpha\frac{\rho_l}{\Delta P}. \tag{8}$$

Then the dimensionless bubble radius and time can be expressed as

$$R^+ = \frac{R}{R_c}, \qquad t^+ = \frac{t}{t_c}. \tag{9}$$

The pressure difference in Eq. (8) cannot be measured. We will use the departing radius as a scaling parameter to adjust the asymptotic growth behavior. The pressure difference can be related to the departing radius, R_d, by the static equilibrium, since radial acceleration and velocity are negligible close to departure (see Eq. (6)). Then, the characteristic scales from Eq. (8) can be rewritten as

$$R_c = \frac{\sqrt{27}}{2} Ja\alpha \sqrt{\frac{\rho_l R_d}{\sigma}}, \qquad t_c = \frac{9}{4} Ja\alpha \frac{\rho_l R_d}{\sigma}. \tag{10}$$

Fig. 8(b) shows the present and previous results scaled using the dimensionless parameters of Eq. (10). There is good agreement between the results.

The latter part of bubble growth was asymptotic proportional to $t^{+1/5}$ in Fig. 8(b). Rayleigh (1917) showed that the growth rate with a constant pressure difference was proportional to t^+, which is reasonable during the initial growth phase. Therefore, we propose a function of dimensionless time t^+ that encompasses the global growth behavior as follows:

$$R^+(t^+) = \alpha t^{+1/5} \tanh(\beta t^{+4/5}) + R_0^+, \tag{11}$$

where α ($=11.2$) and β ($=0.345$) are fitting parameters, which are evaluated using the radius from the experiment. And R_0^+ ($=7.2\times10^{-2}$) is the dimensionless critical radius. The critical radius can be obtained using the Clasius–Clapeyron relation and the Laplace–Kelvin equation for static equilibrium,

$$R_{crit} = \frac{2\sigma T_s}{\rho_v h_{fg} \Delta T}, \tag{12}$$

where, σ is the surface tension, T_s is the saturation temperature, and ΔT is the difference between the wall temperature and the saturation temperature.

Eq. (11) was fitted with the growth data for R11 to analyze the heat transfer characteristics quantitatively using the relation of Eq. (4). Even though the equation was fitted for R11, the suggested equation shows good agreement with the previous results in Fig. 8(b). When the dimensionless time is 10, the value of $\tanh(\beta t^{+4/5})$ becomes 0.97. Thus, the growth behavior becomes asymptotic after that time.

The scattered initial behavior shown in Fig. 8(b) is supposed to be mainly due to the different heating conditions and/or the uncertainties near the inception time. The measured heat flow rate close to departure did not vary significantly (similar to the constant heat flux condition), while there were large variations during the initial growth phase. In addition, there were many uncertainties near inception, such as cavity size, inception time, and heater control. As will be demonstrated in Fig. 10, the characteristic time for the heat flow rate is 10^{-6} s. If the time resolution of the surface condition control is coarser than the characteristic time, the surface condition cannot be maintained at a uniform value throughout the experiment and the growth behavior for each period in a series of experiments will differ.

Even though different boundary conditions and working fluids were used, the dimensionless departure radius was approximately 25, and the dimensionless departure time was approximately

60. Using the values of the dimensionless departure radius and time, the dimensional departure radius and time can be predicted as follows:

$$R_{\mathrm{d}}^{+} = \frac{R_{\mathrm{d}}}{\frac{\sqrt{27}}{2} Ja\alpha \sqrt{\frac{\rho_{\mathrm{l}} R_{\mathrm{d}}}{\sigma}}} = 25, \qquad t_{\mathrm{d}}^{+} = \frac{R_{\mathrm{d}}}{\frac{9}{4} Ja\alpha \frac{\rho_{\mathrm{l}} R_{\mathrm{d}}}{\sigma}} = 60, \tag{13}$$

$$R_{\mathrm{d}} = \left[\frac{25}{2} \sqrt{27} Ja\alpha \sqrt{\frac{\rho_{\mathrm{l}}}{\sigma}} \right]^{2}, \qquad t_{\mathrm{d}} = 135 Ja\alpha \frac{\rho_{\mathrm{l}} R_{\mathrm{d}}}{\sigma}. \tag{14}$$

Fig. 9 shows the comparison of the predicted departure radius and time with the experimental results. The departure radius and time can be predicted with 30% error.

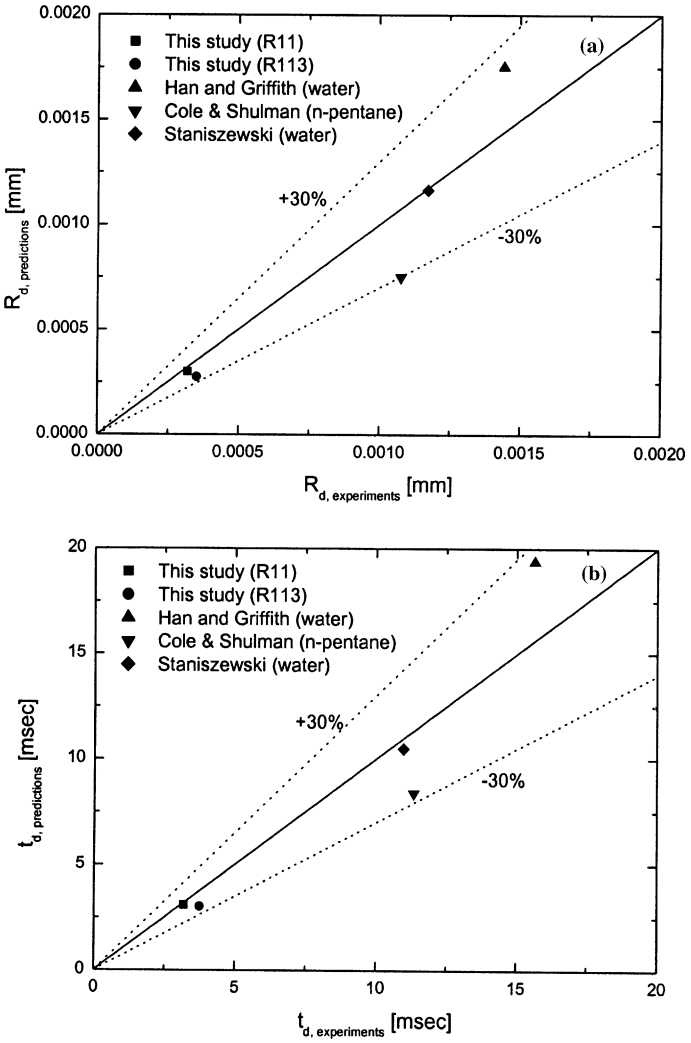

Fig. 9. Comparison of the departure radius and time.

3.3. Heat transfer characteristics

The characteristic scale of the heat flow rate was obtained from Eq. (4), as follows:

$$\dot{q}_c = 4\pi\rho_v h_{fg} R_c^2 \frac{R_c}{t_c}. \tag{15}$$

Using the characteristic scales of Eq. (10), the dimensionless heat flow rate is

$$\dot{q}^+ = \frac{\dot{q}}{\dot{q}_c}, \qquad \dot{q}_c = \frac{54}{\sqrt{3}}\pi\rho_v h_{fg} Ja^2\alpha^2\sqrt{\frac{\rho_l R_d}{\sigma}}. \tag{16}$$

Fig. 10 shows the behavior of the dimensionless heat flow rate for R11. It shows an abrupt increase in the heat flow rate immediately after inception. The slope of the measured heat flow rate is 16, and the time variation for a unit change in the heat flow rate is, therefore, 1/16. The dimensional time variation for the change in the heat flow rate during the initial stage can be evaluated using Eqs. (9) and (10),

$$\Delta t = t_c \Delta t^+ = \frac{9}{4} Ja\alpha \frac{\rho_l R_d}{\sigma} \times \frac{1}{16} \tag{17}$$

Using Eq. (17), the evaluated time variation for the unit change in the heat flow rate is 3.4×10^{-6}. Therefore, the time resolution of the heating control should be greater than this value to maintain accurate control during the rapid increase of the heat flow rate.

For the quantitative analysis for the heat transfer characteristics, the dimensionless equation of Eq. (11) was fitted with the R11 data. It can be converted into the dimensional form, and it is shown as the solid line in Fig. 11(a). Using Eqs. (4) and (11), the required heat flow rate for the observed bubble growth can be calculated. The solid line in Fig. 11(b) represents the required heat flow rate for the bubble growth, and the symbol represents the measured heat flow rate instan-

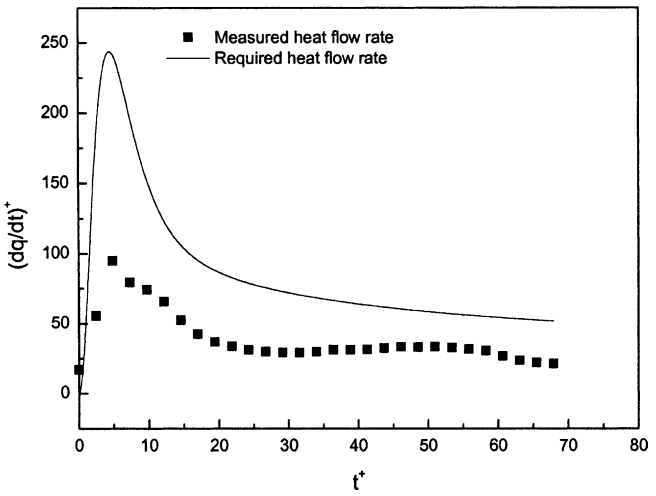

Fig. 10. Non-dimensionalized heat flow rate.

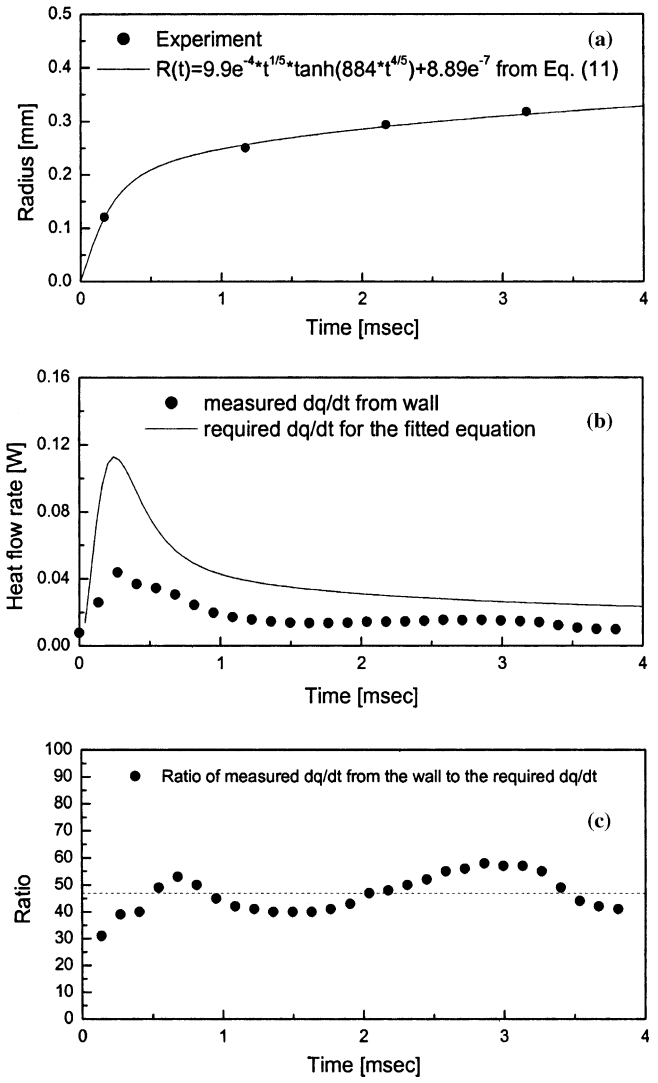

Fig. 11. Comparison of the required heat flow rate and the measured heat flow rate for R11.

taneously supplied from the heating wall. The required heat flow rate shows good qualitative agreement with the measured heat flow rate supplied form the wall. There are deviations, however, between the required heat flow rate and the measured heat flow rate during the growth period. It means that bubble growth requires more heat flow rate than the measured heat flow rate. The additional heat must be supplied through another surface, other than the bottom surface of the bubble. This heat cannot be measured instantaneously, because heat transfer through the liquid from the heating wall requires time. Heat has already been supplied to the liquid during the waiting period before inception and during growth. Fig. 11(c) shows the ratio of the measured heat flow rate supplied from the heating surface to the total heat required for bubble growth. The line in the figure has an average value of 47%.

The contribution of the instantaneous heat supply from the wall was roughly 50% of the required heat for bubble growth (see Fig. 11(c)). Koffman and Plesset (1983) reported that maximum 50% of the heat flow during bubble growth would be transferred by microlayer evaporation. From the bottom view image and the heat flow rate data, we observed that the instantaneous heat was transferred through a narrow region near the contact line. If a microlayer exists underneath the bubble, most of the measured heat flow rate supplied from the wall will be transferred by microlayer evaporation.

The additional heat that is the difference between the required heat flow rate and the measured heat flow rate should be supplied through another surface, other than the bottom surface of the bubble. During bubble growth, the heat supplied to the bubble can be roughly divided into two parts: the instantaneous and *direct* supply through the heating wall, and the *indirect* supply from the preheated liquid near the heating surface. The former can be measured with the present device; however, the latter must be modeled. The *indirect* heat supply is related to the non-uniform temperature field around the bubble interface. The effects of the waiting period and non-uniform temperature field were analyzed by Mikic and Rohsenow (1969), but the interface temperature variation was neglected (or considered negligible) by assuming that the vapor pressure did not vary with time. Recently, Robinson and Judd (2001) evaluated vapor pressure using the extended Rayleigh equation. The non-uniform temperature field was computed by solving the energy equation numerically. A temperature gradient developed around the interface and heat was supplied at a very high rate, due to the rapid decrease of the vapor pressure. Such a heat transfer mechanism is termed the interface cooling effect, and can explain the *indirect* heat supply through the bubble interface.

The heat transfer through the thermal boundary layer around the bubble would be enhanced by the interface cooling effect. It could be predicted using the fitted growth equation that the rapid decrease of the interface temperature was ended around 1 ms, but it is supposed that the thermal boundary layer that had been developed around the bubble interface by the wall heating and the rapid decrease of the interface temperature would exist still after the time. As time goes, the temperature difference of the thermal boundary layer decreases, and the absolute value of the heat flow rate decreases, as shown in Fig. 11(b).

4. Conclusions

A quantitative analysis for a single bubble's growth in saturated nucleate pool boiling with a constant wall temperature was performed. The wall temperature was controlled precisely using a microscale heater array, and the local heat flow rate was measured at a high temporal resolution. Time-triggered high-speed CCD images were captured at a sampling rate of 1000 Hz for R11 and 4000 Hz for R113 to analyze bubble motion.

The captured images showed an spheroidal-shaped bubble during the growth. The captured images showed an asymptotic bubble growth rate proportional to $t^{1/5}$, which was slower than that of previous analytic analyses. The measured heat flow rate showed good repeatability and a discernable peak in the initial growth stage. It reached almost constant value.

Bubble growth behavior during saturated pool boiling was analyzed using a new dimensionless parameter. Dimensionless parameters of time and bubble radius characterized the asymptotic

growth behavior well, irrespective of the wall condition. A comparison between the present and previous results showed good agreement during the asymptotic growth region. The dimensionless departure time was approximately 60, the dimensionless departure radius was approximately 25, and the dimensionless time at which the bubble started to grow asymptotically was approximately 10.

A growth equation that predicts the $R \propto t$ growth behavior during the initial stage and the $R \propto t^{1/5}$ growth behavior in the asymptotic region was suggested using a transcendental function of tanh: $R^+(t^+) = 11.2t^{+1/5}\tanh(0.345t^{+4/5}) + 7.2 \times 10^{-2}$. The heat flow rate behavior evaluated using the equation showed good qualitative agreement with the measured heat flow rate supplied from the wall, but there was a difference between the required heat flow rate and the measured heat flow rate. The difference can be explained with the heat transfer through the thermal boundary layer around the bubble surface.

Acknowledgements

This work was supported by the Ministry of Science and Technology of Korea through the National Research Laboratory program. The authors are grateful to Prof. Jungho Kim for providing the basic design of the microscale heater array, including its controller, and to the Samsung Advanced Institute of Technology for fabricating the microscale heater array.

References

Bae, S.W., Kim, J., Kim, M.H., 1999. Improved technique to measure time- and space-resolved heat transfer under single bubbles during saturated pool boiling of FC-72. Exp. Heat Transfer 12, 265–279.

Cole, R., Shulman, H.L., 1966. Bubble growth rates at high Jakob numbers. Int. J. Heat Mass Transfer 9, 1377–1390.

Coleman, H.W., Steele Jr., W.G., 1989. Experimentation and Uncertainty Analysis for Engineers. John Wiley & Sons Inc, New York, USA.

Dhir, V.K., 1998. Boiling heat transfer. Annu. Rev. Fluid Mech., 365–401.

Forster, H.K., Zuber, N., 1954. Growth of a vapor bubble in a superheated liquid. J. Appl. Phys. 25, 474–478.

Han, C.H., Griffith, P., 1965. The mechanism of heat transfer in nucleate pool boiling—Part I Bubble initiation, growth and departure. Int. J. Heat Mass Transfer 8, 887–904.

Kim, J., Benton, J.F., 2002. Highly subcooled pool boiling heat transfer at various gravity levels. Int. J. Heat Fluid Flow 23, 497–508.

Kim, J., Benton, J.F., Wisniewski, D., 2002. Pool boiling heat transfer on small heaters: effect of gravity and subcooling. Int. J. Heat Mass Transfer 45, 3919–3932.

Koffman, L.D., Plesset, M.S., 1983. Experimental observation of the microlayer in vapor bubble growth on a heated solid. J. Heat Transfer 105, 625–632.

Lee, H.S., Merte Jr., H., 1996. Spherical vapor bubble growth in uniformly superheated liquids. Int. J. Heat Mass Transfer 39, 2427–2447.

Mikic, B.B., Rohsenow, W.M., 1969. Bubble growth rates in non-uniform temperature field. Prog. Heat Mass Transfer II, 283–293.

Mikic, B.B., Rohsenow, W.M., Griffith, P., 1970. On bubble growth rates. Int. J. Heat Mass Transfer 13, 657–666.

Plesset, M.S., Zwick, S.A., 1954. The growth of vapor bubbles in superheated liquids. J. Appl. Phys. 25, 493–500.

Rayleigh, J.W.S., 1917. On the pressure developed in a liquid during the collapse of a spherical cavity. Philos. Mag. 34, 94–98.

Robinson, A.J., Judd, R.L., 2001. Bubble growth in a uniform and spatially distributed temperature field. Int. J. Heat Mass Transfer 44, 2699–2710.

Rule, T.D., Kim, J., 1999. Heat transfer behavior on small horizontal heaters during pool boiling. J. Heat Transfer 121, 386–393.

Rule, T.D., Kim, J., Kalkur, T.S., 1998. Design, construction and qualification of a microscale heater array for use in boiling heat transfer. NASA/CR-1998-207407.

Staniszewski, B.E., 1959. Nucleate boiling bubble growth and departure. M.I.T. DSR Project No. 7-7673, Technical Report No. 16.

Van Stralen, S.J.D., 1966. The mechanism of nucleate boiling in pure liquids and in binary mixtures—Part I. Int. J. Heat Mass Transfer 9, 995–1020.

Zuber, N., 1961. The dynamics of vapor bubbles in nonuniform temperature fields. Int. J. Heat Mass Transfer 2, 83–98.